Cerebral Cortex, February 2020;30: 451–464

doi: 10.1093/cercor/bhz096
Advance Access Publication Date: 18 June 2019
Original Article

ORIGINAL ARTICLE

Altered Sensitivity to Motion of Area MT Neurons Following Long-Term V1 Lesions

Maureen A. Hagan[1,2,3], Tristan A. Chaplin[1,2,3,4], Krystel R. Huxlin[5], Marcello G. P. Rosa[1,2,3] and Leo L. Lui[1,2,3]

[1]Department of Physiology, Monash University, Clayton, VIC 3800, Australia, [2]Neuroscience Program, Biomedicine Discovery Institute, Monash University, Clayton, VIC 3800, Australia, [3]Australian Research Council, Centre of Excellence for Integrative Brain Function, Monash University Node, Clayton, VIC 3800, Australia, [4]Sainsbury Wellcome Centre for Neural Circuits and Behaviour, University College London, 25 Howland Street, London W1T 4JG, United Kingdom and [5]Flaum Eye Institute, University of Rochester, Rochester, NY 14642, USA

Address correspondence to Leo L. Lui, Department of Physiology, Monash University, Clayton, VIC 3800, Australia. Email: Leo.Lui@monash.edu.
http://orcid.org/0000-0001-9762-0457

Abstract

Primates with primary visual cortex (V1) damage often retain residual motion sensitivity, which is hypothesized to be mediated by middle temporal area (MT). MT neurons continue to respond to stimuli shortly after V1 lesions; however, experimental and clinical studies of lesion-induced plasticity have shown that lesion effects can take several months to stabilize. It is unknown what physiological changes occur in MT and whether neural responses persist long after V1 damage. We recorded neuronal responses in MT to moving dot patterns in adult marmoset monkeys 6–12 months after unilateral V1 lesions. In contrast to results obtained shortly after V1 lesions, we found that fewer MT neurons were direction selective, including neurons expected to still receive projections from remaining parts of V1. The firing rates of most cells increased with increases in motion strength, regardless of stimulus direction. Furthermore, firing rates were higher and more variable than in control MT cells. To test whether these observations could be mechanistically explained by underlying changes in neural circuitry, we created a network model of MT. We found that a local imbalance of inhibition and excitation explained the observed firing rate changes. These results provide the first insights into functional implications of long-term plasticity in MT following V1 lesions.

Key words: blindsight, marmoset monkey, motion, MT, plasticity, vision

Introduction

Damage to the primary visual cortex (V1) in adult primates leads to loss of conscious visual perception (Lister and Holmes 1916). In cases of partial destruction, a defined scotoma (an "island" of blindness) is created, which precisely follows the topographic representation of the visual field in V1 (Horton and Hoyt 1991). Despite the absence of visual sensation, humans and monkeys with V1 lesions sustained in adulthood often retain a residual ability to respond to moving or flickering visual stimuli within the scotomas (Riddoch 1917; Klüver 1936, 1941; Poppel et al. 1973; Sanders et al. 1974; Barbur et al. 1993; Weiskrantz 1996).

The middle temporal (MT) area of extrastriate cortex is a likely neural substrate for mediating the residual visual motion

processing. While MT receives most of its input from V1 (Palmer and Rosa 2006), it also receives inputs from subcortical (Stepniewska et al. 2000; Sincich et al. 2004; Kaas and Lyon 2007; Warner et al. 2010) and other cortical (Weller et al. 1984; Palmer and Rosa 2006; Schmid et al. 2013) areas that could mediate responses in MT in the absence of V1 input. It has been shown that, within weeks of V1 lesions, a population of MT neurons still responds in a direction selective way to oriented bars and gratings presented inside the scotoma (Rodman et al. 1989; Rosa et al. 2000; Azzopardi et al. 2003; Alexander and Cowey 2008).

However, after loss of sensory input, the cortex continues to undergo changes, resulting in neural plasticity over several months post-damage (Kaas et al. 1990; Darian-Smith and Gilbert 1994; Yamahachi et al. 2009). Lateral excitatory connections, which can extend several millimeters across the cortex linking cells with non-overlapping receptive fields (Darian-Smith and Gilbert 1994; Stettler et al. 2002), increase in density both within and across the lesion projection zone (LPZ; the region of cortex that originally received afferent connections from the lesioned tissue) (Darian-Smith and Gilbert 1994; Palagina et al. 2009; Yamahachi et al. 2009; Barnes et al. 2017). This increase in excitatory connections is believed to cause the receptive fields of cells inside the LPZ to shift outwards, toward the border of the scotoma (Yamahachi et al. 2009). This receptive field shift has been widely observed in cortex after loss of sensory input (Eysel et al. 1999; Giannikopoulos and Eysel 2006), including in MT after V1 damage (Rosa et al. 2000). Furthermore, the connectivity of inhibitory neurons within the LPZ decreases (Keck et al. 2011). This imbalance in excitation and inhibition can lead to hyper-excitation in cortical tissue after loss of sensory input (Giannikopoulos and Eysel 2006). The effects of such plasticity on the long-term response properties of MT neurons have not been investigated.

Humans with V1 damage exhibit the greatest rates of visual recovery without therapeutic intervention within the first weeks after their lesion, with spontaneous improvements occasionally seen up to 6 months post-V1 damage. Once patients reach 6 months post-V1 damage, spontaneous improvement ceases (Zhang et al. 2006). The response properties of MT cells, such as sensitivity to direction of motion and motion coherence, have not been investigated at this later time point. Understanding how neuronal responses change with time post-lesion is critical for understanding how plasticity in the adult visual system might evolve after damage, as the system first heals and then adapts to its new state.

To address these questions, we recorded the response properties of MT neurons to moving random dot patterns in marmoset monkeys 6–12 months following V1 lesions. Although MT neurons still responded to these stimuli long after V1 lesions, we found that firing rates, as well as sensitivity to direction of motion and motion coherence, were significantly altered. To test whether changes in MT responses could be explained by underlying changes in neural plasticity, we implemented a network model of MT. We were able to demonstrate that the observed changes in neural responses were consistent with increased lateral excitatory connectivity and decreased inhibition.

Materials and Methods

Animals and Surgical Preparation

Single and multi-unit extracellular recordings were obtained from 6 adult common marmosets (*Callithrix jacchus*, 3 males and 3 females). Experiments were conducted in accordance with the Australian Code of Practice for the Care and Use of Animals for Scientific Purposes, and all procedures were approved by the Monash University Animal Ethics Experimentation Committee. Four of the marmosets received V1 lesions (M1 to M4) between 26–34 months of age (see Table 1). Electrophysiological recordings were performed at least 6 months after the V1 lesion. Data were obtained from 2 additional adult marmosets (M5, M6) with no V1 lesions.

Table 1 Summary of animal ages at time of lesion and neural recordings

Animal ID	Sex	Age in months at time of V1 lesion	Neural recording	Months post-lesion
M1	M	34	45	11
M2	F	26	38	12
M3	F	33	40	7
M4	F	26	32	6

Data for each V1-damaged animal (M1 to M4) showing sex, age at time of V1 lesion, and neural recordings.

Cortical Lesions

Intramuscular (i.m.) injections of atropine (0.2 mg/kg) and diazepam (2 mg/kg) were administered as premedication, 30 min prior to the induction of anesthesia with alfaxalone (Alfaxan, 10 mg/kg, Jurox). Dexamethasone (0.3 mg/kg i.m., David Bull) and penicillin (Norocillin, 50 mg/kg, i.m.) were also administered. Body temperature, heart rate, and blood oxygenation ($SP0_2$) were continually monitored, and supplemental doses of anesthetic were administered when necessary to maintain areflexia. Under sterile conditions, a craniotomy was made over the occipital pole of the left hemisphere. Using a fine-tipped cautery, an excision was then made of all cortical tissue caudal to a plane extending from the dorsal surface of the occipital lobe to the cerebellar tentorium, across the entire mediolateral extent (Rosa et al. 2000). The caudal 6–8 mm of cortex (approximately two-thirds of V1) was removed entirely, including the occipital operculum, the exposed medial and ventral surfaces, and the caudal part of the calcarine sulcus (Fig. 1A–C). After the application of hemostatic microspheres, the exposed cortex and cerebellum were protected with ophthalmic film, and the cavity was filled with Gelfoam. The skull flap was repositioned and secured with cyanacrylate (Vetabond, 3M), the skin was sutured, and antibiotics (Norocillin, 50 mg/kg, i.m.) and analgesics (Buprenorphin, 0.01 mg/kg, i.m.) were given. Following the V1 lesion surgery, animals recovered for 6–12 months before electrophysiological recordings (see Table 1). Throughout the post-lesion period, monkeys were housed in large cages in groups with access to both indoor and outdoor environments.

Electrophysiological Recordings

The preparation for electrophysiological studies of marmosets has been described previously (Yu et al. 2010), and only the main points will be summarized here. Injections of atropine (0.2 mg/kg, i.m.) and diazepam (2 mg/kg, i.m.) were administered as premedication, 30 min prior to the induction of anesthesia with alfaxalone (Alfaxan, 10 mg/kg, i.m., Jurox), allowing a tracheotomy, vein cannulation, and craniotomy to be per-

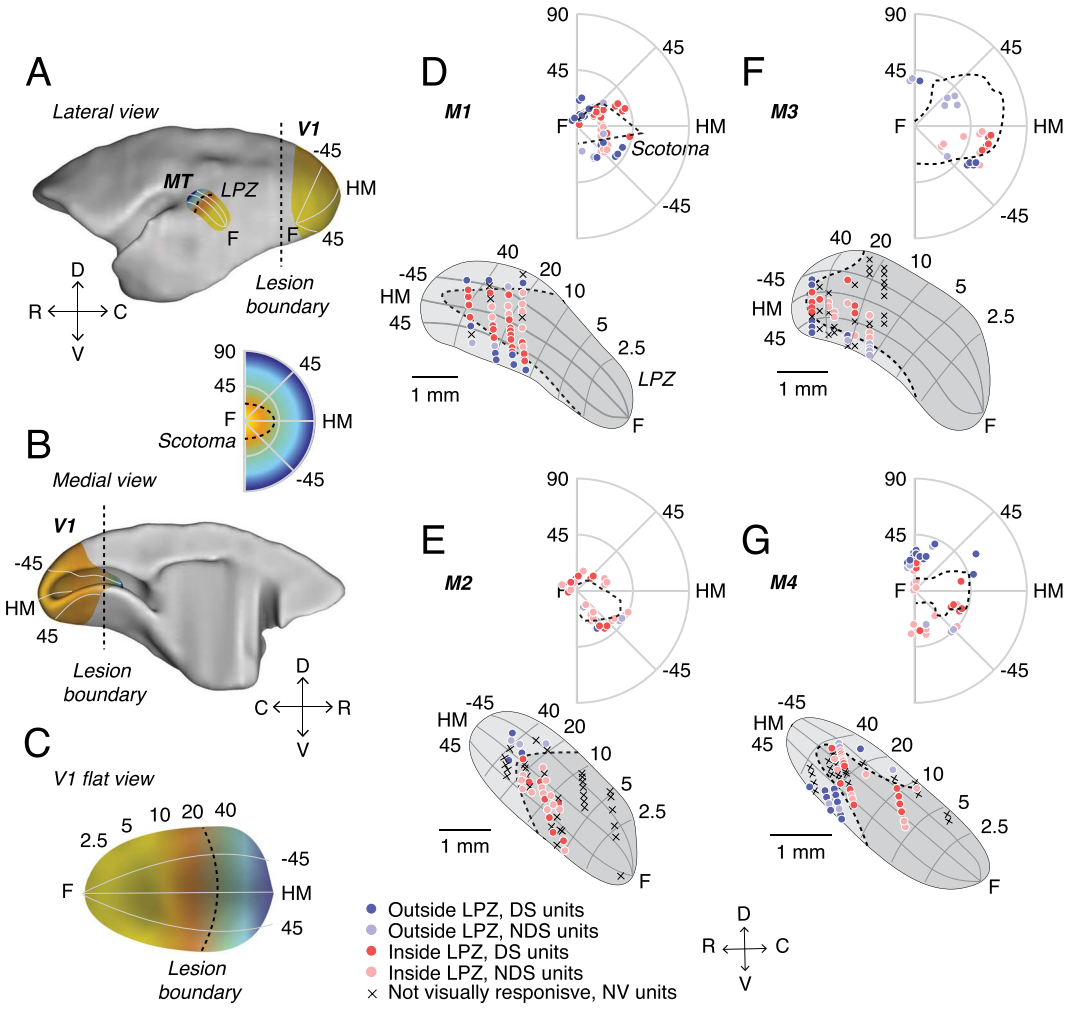

Figure 1. V1 lesions in adult marmosets. (*A*) Lateral and (*B*) medial views of a marmoset brain showing the locations of V1 and MT, as well as a C, flat view of V1. Illustrative retinotopic maps have foveal responses in yellow and peripheral responses in blue. Dashed lines illustrate the approximate location of the lesion boundary in V1 (*A–C*) and the corresponding LPZ in MT (*A*) and scotoma in the visual field (inset). (*D–G*) Anatomical locations of units recorded from MT and their respective receptive fields locations in the visual field in 4 adult marmosets (M1 to M4, respectively) with V1 lesions. V1 recordings were used to define the boundary of the scotoma in each V1-damaged animal, and the scotoma was then projected onto the cortical surface representation of MT (see Methods) in order to determine the LPZ for each case. Each point indicates the recording location of a unit in MT (below) or one stimulus center in the visual field map (above). Dark colors indicate direction selective (DS) units; light circles indicate units that were visually responsive but not direction selective (NDS). Red points indicate units recorded inside the LPZ and blue points indicate units outside the LPZ. Crosses indicate units that were not visually responsive (NV). Dashed lines indicate the LPZ in MT and the scotoma in the visual field. Numbers (degrees) indicate eccentricity (vertical axis) and polar angle (radial axes). The dashed lines indicate LPZ in MT and scotoma in visual field. C, caudal; D, dorsal; R, rostral; V, ventral; F, fovea; HM, horizontal meridian.

formed. After all surgical procedures were completed, the animal received an intravenous infusion of pancuronium bromide (0.1 mg/kg/h; Organon) combined with sufentanil (6 µg/kg/h; Janssen-Cilag) and dexamethasone (0.4 mg/kg/h; David Bull) and was artificially ventilated with a gaseous mixture of nitrous oxide and oxygen (7:3). The electrocardiogram and level of cortical spontaneous activity were continuously monitored. Administration of atropine (1%) and phenylephrine hydrochloride (10%) eye drops (Sigma Pharmaceuticals) resulted in mydriasis and cycloplegia. Appropriate focus and protection of the corneas from desiccation were achieved by means of hard contact lenses selected by streak retinoscopy.

Neural recordings were made using single parylene-coated tungsten microelectrodes (0.7–1.2 MΩ) with exposed tips of 10 µm (Microprobe). Electrophysiological data were recorded using a Cereplex system (Blackrock Microsystems) with a sampling rate of 30 kHz. Each channel was high-pass filtered at 750 Hz. Spike waveforms were extracted offline at a threshold of 3.5 standard deviations (SDs) below the median voltage. Spike waveforms were then over-clustered using principal component analysis to identify single-unit activity. Any remaining threshold crossings were classified as multi-unit activity.

Experimental Design and Statistical Analysis

Stimuli

Computer-generated stimuli were presented on a Display++ monitor (M1 to M4; 1920 × 1080 pixels; 710 × 395 mm; 120 Hz refresh rate, Cambridge Research Systems) or a VIEWPixx3D monitor (M5 and M6; 1920 × 1080 pixels; 520 × 295 mm; 120 Hz refresh rate, VPixx Technologies) positioned 0.35–0.45 m from the animal at an angle that allowed stimulation of 76–90 degrees

of the visual field along the horizontal meridian. All stimuli were generated with MATLAB using Psychtoolbox-3 (Brainard 1997; Pelli 1997).

Stimuli for quantitative analysis consisted of random dots presented in circular apertures. Dots were white and displayed on a black background and were 0.2 deg in diameter. The density was such that there were on average 0.5 dots per deg^2. Dot coherence was controlled by randomly choosing a subset of "noise" dots on each frame that were displaced randomly within the stimulus aperture. The remaining "signal" dots were moved in the same direction with a fixed displacement (Britten et al. 1992).

Determination of the Physiological Scotoma

The location of the scotoma in lesioned animals was determined by mapping the receptive fields of neurons in the remaining parts of V1, near the border of the lesions (Fig. 1*D*–*G*). This was done either on the Display++ monitor, using static flashed squares (M1), or by hand mapping with luminance-defined stimuli on a hemispheric screen (Yu and Rosa 2010). As reported elsewhere (Rosa et al. 2000; Yu et al. 2013), the locations of receptive fields of neurons located on both the dorsal and ventral banks of the calcarine sulcus were similar to those found at corresponding locations in normal animals (Fritsches and Rosa 1996; Chaplin et al. 2013). The physiological scotoma (i.e., the part of the visual field no longer represented in V1) was defined as the area of the visual field in which V1 receptive fields could no longer be recorded (Fig. 1*D*–*G*; dashed outlines).

Determination of MT Receptive Fields

In MT, receptive fields were quantitatively mapped using a grid of stimuli presented across the screen. These stimuli were either small apertures of briefly presented moving dots (300 ms, diameter 5 degrees, animals M1 to M4) or static flashed squares (length 4 degrees, animals M5 and M6). For quantitative tests, stimuli were presented inside a circular aperture restricted to the excitatory receptive field.

Quantitative Tests

We conducted a series of tests to determine direction selectivity, speed tuning, and sensitivity to motion coherence. All stimuli were presented for 500 ms with an inter-stimulus interval of 1000 ms. Direction and speed tuning tests used at least 12 repeats of each stimulus type, and motion coherence tests used 25 repeats.

We tested for direction selectivity by presenting a circular aperture of random dots that moved in 1 of 8 directions (0, 45, 90, 135, 180, 225, 270, 315) at 8 deg/s. Speed tuning was then tested using random dot stimuli with speeds (0, 2, 4, 8, 16, 32, 64, 128 deg/s) moving in the preferred and null direction. Stimuli with different motion coherences (0, 5, 10, 20, 50, 75, 100%) were presented at a near-preferred speed, in both preferred and null directions.

In 2 animals (M2 and M3) we additionally used a sinusoidal grating stimulus to test direction selectivity. Gratings were presented in a circular aperture at high contrast on a gray background. In M2, first the preferred temporal frequency was found (0.5, 1, 2, 4, 8 cycles/s) at 0.2 cycles/deg, followed by a test to find the preferred spatial frequency (0.05, 0.1, 0.2, 0.4, 0.8 cycles/deg). In M3, all spatial and temporal frequencies were randomly interleaved. In both animals, direction selectivity was tested at the preferred spatial and temporal frequency for each unit.

Visual Response

Neurons were considered to be visually responsive if the mean stimulus-evoked activity across all conditions was significantly greater than the spontaneous rate (Wilcoxon rank sum test, $P < 0.05$).

Direction Selectivity

The preferred direction was calculated using a vector sum of normalized above-spontaneous spiking rates (Ringach et al. 2002). In each task, neurons were classified as direction selective if the response in the preferred direction was significantly greater than the null direction (Wilcoxon rank sum test, $P < 0.05$). To measure the degree of direction selectivity, we used 3 metrics.

First, we calculated a direction selectivity index (DSI):

$$\mathrm{DSI} = 1 - \frac{R_{null}}{R_{pref}}, \tag{1}$$

where R_{pref} and R_{null} are the above spontaneous spike rates in the preferred and null directions, respectively. Circular variance (CV) was calculated as 1 minus the length of the vector sum of normalized above-spontaneous spiking rates (Ringach et al. 2002). We also employed ideal observer analysis to determine the performance of MT neurons in discriminating 2 directions (Britten et al. 1992). This was calculated using the Receiver Operator Characteristic (aROC) curve for the distributions of responses to the preferred and null directions.

z-Score Firing Rate Differences

We used random permutation to determine if the difference in mean between 2 conditions was significantly different than a distribution of mean differences from trials that were shuffled and chosen at random. We repeated this permutation 10 000 times to obtain a distribution.

Direction Thresholds

In order to quantify a unit's susceptibility to motion noise, we employed ideal observer analysis to determine performance of MT neurons in a direction discrimination task (Britten et al. 1992). For each level of coherence, aROC was calculated, and the aROC values were fitted using least squares regression with a Weibull function, resulting in a neurometric curve that described the neuron's performance with respect to coherence.

$$P = 1 - 0.5\ \exp\left[-(c/\alpha)^{\beta}\right], \tag{2}$$

where P was the probability of correctly discriminating the direction of motion at coherence c, α was the coherence of threshold performance ($P = 0.82$), and β controls slope. The α was limited between 0 and 3, and the β was limited to be between 0 and 10. Neurons that do not have an aROC of at least 0.82 at 100% coherence cannot have a threshold (i.e., $P(c = 100) < 0.82$) and were excluded from analyses of thresholds, as was any neuron whose threshold exceeded 100%.

Motion Thresholds

In order to determine how well neurons could detect motion in the preferred direction versus random motion, we calculated aROC comparing the distribution of spikes evoked by each level of motion coherence with the distribution of spikes evoked by zero coherence. As for direction thresholds, we fit a Weibull

function (equation (2) above) to these data to determine the detection threshold.

Mean-Matched Fano Factor

To compute the variance in firing rates over time, we computed the mean-matched Fano factor using the procedures described by Churchland et al. (2010) using the Variance toolbox (Stanford University) in MATLAB. Briefly, for each single unit we used the firing rates from the motion coherence task. Each stimulus condition (motion coherence and direction) was treated separately. Spike counts were computed using a 100 ms sliding window moving in 50 ms time steps. To control for differences in firing rates, we computed a mean-matched Fano factor. For each time window, we matched the mean firing rates by randomly deleting spikes until mean rates were matched across time. The Fano factor was then computed from the residual spikes.

Network Model

We implemented a network model of our data in Python using the Brian simulator version 2. The network model was a biophysical network model of a randomly connected excitatory/inhibitory (E/I) network with 1600 excitatory (E) and 400 inhibitory (I) leaky integrate-and-fire neurons. We used the Euler integration method with a time step of 0.1 ms. The network model was based on the model of an MT-like sensory circuit published by Wimmer et al. (2015). All model equations and parameter values used were replicated from Wimmer et al. (2015). Synaptic transmission mimicked AMPA and $GABA_A$ receptor conductance dynamics. Excitatory neurons were divided into 2 populations, E1 and E2, each preferring opposite directions of motion. Connections within each population were stronger ($w_{pref} = 1.1$) compared with connections across populations ($w_{null} = 0.9$), mimicking the stronger coupling among cells with similar tuning. The 2 populations were then further divided into 2 equal sub-populations (E1i, E2i, E1o, E2o) that represented cells inside and outside the LPZ. Neurons inside the LPZ were subjected to changes probability excitatory and inhibitory connections.

The input into MT was modeled as a time-varying input current into each neuron:

$$I_{stim,k}(t) = V_i\,(1 + cD_i + s(t))\,, \tag{3}$$

where I_{stim} is the amount of current (nA) injected into each neuron (k) at over time (t). V_i is the amount of visual input for a stimulus regardless of motion coherence (0.04 nA). D_i is the amount of additional direction selective input to a neuron when the stimulus is moving in the preferred direction and is modulated by the motion coherence (c) of the stimulus. Time-varying modulations in sensory input by the specific realization of the random dot stimulus are captured by $s(t)$ where

$$s(t) = \sigma_s z^{\beta}(t) + \sigma_s z_k^{\beta}(t), \tag{4}$$

where $z^{\beta}(t)$ and $z_k^{\beta}(t)$are independent Ornstein–Uhlenbeck processes with zero mean, SD equal to one, and a time constant of 20 ms. The term $z^{\beta}(t)$ represents the "common" part of the stimulus that is consistent across each neural population β, and $z_k^{\beta}(t)$ represents the "private" part of the stimulus that is unique to each neuron in each population. The amplitude of the temporal modulation of the stimulus is set by σ_s (0.212). We tested stimuli at 5 motion coherences (0, 25, 50, 75, 100%) in the preferred directions of E1 and E2 (9 conditions total). As in the experimental conditions, the "stimulus" lasted for 500 ms with a 1000 ms interval between repetitions. Each motion coherence and direction was randomly interleaved and presented 20 times per condition.

We modified the E/I balance of the network by manipulating the probability of synaptic connections between neurons. In the control condition, all neural connections (EE, EI, II) were connected with equal probability ($P = 0.2$). We then assigned half the cells in the population as being "inside" the LPZ and the other half as "outside" the LPZ. The probability of excitatory connections was increased for in cells inside the LPZ ($P = 0.3$). This was true for connections within and across the LPZ, to mimic the changes observed in lateral excitatory projections that have been observed. The probability of connection with inhibitory neurons inside the LPZ was also decreased ($P = 0.1$). Finally, we set the weighting of synaptic inputs between excitatory neurons inside and outside the LPZ ($w = 1.1$).

As an alternative to an E/I imbalance, we also tested the effect of a change of input into the LPZ. In this case, all neural connections (EE, EI, II) were connected with equal probability ($P = 0.2$), as in control conditions. Neurons inside the LPZ received a visual, non-direction selective input ($D_i = 0$, equation (3)).

Histology

At the end of the recordings (2–3 days) the animals were given an intravenous lethal dose of sodium pentobarbitone and, following cardiac arrest, were perfused with 0.9% saline, followed by 4% paraformaldehyde in 0.1 M phosphate buffer pH 7.4. The brain was post-fixed for approximately 24 h in the same solution and then cryo-protected with fixative solutions containing 10%, 20%, and 30% sucrose. The brains were then frozen and sectioned into 40 µm coronal slices. Alternate series were stained for Nissl substance and myelin (Gallyas 1979). The location of recording sites was reconstructed by identifying electrode tracks, depth readings recorded during the experiment, and by electrolytic lesions performed at the end of penetrations. Area MT was defined by heavy myelination (Rosa and Elston 1998). Recording sites were projected onto layer 4 lateral view reconstructions of MT (Fig. 2). All neurons reported here were histologically confirmed to be in MT including those in the 2 control animals.

Estimation of LPZ

To assess the changes in responses of in MT of V1-damaged animals compared with control animals, it was necessary to estimate the portion of MT that originally represented the same part of the visual field as the portion of V1 affected by the lesion. This portion of MT is referred to as the LPZ, as neurons inside the LPZ no longer receive normal inputs from V1 after the lesion. To establish the LPZ, isoeccentricity and polar lines were projected onto the lateral view reconstructions of MT in each individual case based on the average visuotopic map of this area (Fig. 1D–G; Rosa and Elston 1998). This average map was based on reconstructions of MT in 6 normal cases, which were superimposed after having been aligned and scaled to equal area. The visuotopy of MT has been demonstrated to be highly consistent across individuals (Rosa and Elston 1998). The estimates of the pre-lesion visuotopic maps thus obtained were then fine-tuned for each case based on the size and extent of MT measured in each case (see above). Based on the visuotopic coordinates, the borders of the scotomas for each individual animal

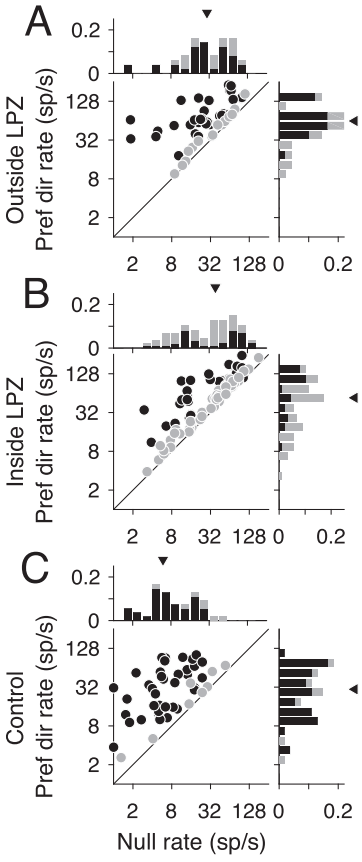

Figure 2. Firing rate differences in V1-damaged and control animals. (*A–C*) Firing rates in the null direction (*x*-axis) compared with preferred (*y*-axis) for units located outside the LPZ ($n = 49$ units), inside the LPZ ($n = 87$ units), and for the 2 control animals ($n = 54$ units), respectively. Darker circles indicate direction selective units; lighter circles indicate non-direction selective units. Histograms show the distribution of firing rates for each axis. Darker bars indicate direction selective units; lighter bars indicate non-direction selective units. Triangles indicate the median rate.

were then projected onto the lateral view reconstructions of MT (Fig. 1*D–G*), thus defining an LPZ for each individual case.

Results

Neural Responsiveness in MT after V1 Lesions

The caudal portion of V1 was resected unilaterally in 4 adult marmosets (Fig. 1*A–C*; see Methods), which resulted in a corresponding LPZ in MT (Fig. 1*A,D–G*) and physiological scotoma in the visual field (Fig. 1 inset, *D–G*); for simplicity, these will be referred to as scotomas henceforth in this paper. The scotomas were elongated in shape, encompassed the central visual field, and extended to at least 40° eccentricity in the right visual hemifield along the horizontal meridian (Fig. 1*D–G*).

We recorded 114 single units and 134 multi-units from MT in 4 V1-damaged animals and 36 single units and 38 multi-units from 2 control animals. As there were no systematic differences between single and multi-unit activity, they have been combined in further analysis and referred to as "units." However, in key analyses the effects on single units are shown separately below. The majority of MT units in V1-damaged animals, both inside (73.3%, 115/157 units) and outside (79.1%, 72/91 units) the LPZ, responded to moving dot patterns. However, the remaining units showed no visual responses and were excluded from further analysis. Among the units that were visually responsive, we found direction selective units in MT in all 4 animals, both inside and outside the LPZ (Fig. 1*A–D*). However, direction selectivity was less prevalent than in control animals. As expected, the majority of units in control animals were direction selective (69.4%, 50/72 visually responsive units), comparable to previous reports using random dot moving patterns in marmosets (Chaplin et al. 2017). Significantly fewer MT units were direction selective in animals with a V1 lesion. Surprisingly, this was true outside the LPZ (59.7%, 43/72 units, $P = 0.02$, Binomial distribution) as well as inside (45.2%, 52/115 units, $P = 3.87 \times 10^{-8}$), although the prevalence of direction selective units was higher outside than inside the LPZ ($P = 5.50 \times 10^{-4}$). The majority of units (85.2%, 98/115 units) located inside the LPZ (which were expected to have receptive fields inside the scotomas according to the normal retinotopic organization of MT) had receptive fields displaced to the borders of the scotoma (Fig. 1 inset, *A–D*).

MT Firing Rates Are Higher and More Variable after V1 Lesions

Metrics of direction selectivity and motion selectivity are dependent on the firing rates of units (Chaplin et al. 2017). If loss of V1 input reduces the overall firing rate of units inside the LPZ, this factor could account for the reduced prevalence of direction selectivity in MT. In fact, we found that firing rates were significantly higher in V1-damaged animals compared with controls—in contrast with previous reports in macaques and marmosets, following shorter survival times (Rodman et al. 1989; Rosa et al. 2000; Azzopardi et al. 2003). MT units in V1-damaged animals had higher firing rates in response to motion in the preferred and null directions as well (Fig. 2*A*, Outside LPZ: median preferred rate = 63.5 sp/s, $P = 3.28 \times 10^{-6}$, median null rate = 32.5 sp/s, $P = 7.07 \times 10^{-10}$; Fig. 2*B*, Inside LPZ: median preferred rate = 81.1 sp/s, $P = 1.65 \times 10^{-4}$, median null rate = 42.6 sp/s, $P = 3.52 \times 10^{-11}$, Wilcoxon's rank sum) compared with units in control animals (Fig. 2*C*, median preferred rate = 35.8 sp/s, median null rate = 5.8 sp/s). Spontaneous rates were also significantly higher outside the LPZ (median spontaneous rate = 11.9 sp/s, $P = 6.72 \times 10^{-8}$) as well as inside the LPZ (median spontaneous rate = 14.2 sp/s, $P = 3.51 \times 10^{-9}$; Control: median spontaneous rate = 4.0 sp/s; data not shown).

While firing rates were generally higher in multi-units compared with single units, firing rates were still significantly higher when considering single units alone (see Supplementary Fig. S1*A*, Outside LPZ: median preferred rate = 51.7 sp/s, $P = 0.03$, median null rate = 19.3 sp/s, $P = 3.50 \times 10^{-4}$; see Supplementary Fig. S1*B*, Inside LPZ: median null rate = 14.7 sp/s, $P = 2.10 \times 10^{-3}$; see Supplementary Fig. S1*C*, Control: median preferred rate = 31.2 sp/s, median null rate = 5.8 sp/s), except firing rates in the preferred direction inside the LPZ, which were not significantly different than controls (see Supplementary Fig. S1*B*, median preferred rate = 29.8 sp/s, $P = 0.68$). Therefore, the lack of direction selectivity was not due to a decrease in the firing rate of units in V1-damaged animals. Rather, the reduced direction selectivity was driven by increased firing rates in the null direction. These results may be consistent with a local loss of inhibition, which has been shown to decrease direction selectivity in MT (Thiele et al. 2004).

In addition to analyzing the mean firing rate, we calculated the mean-matched Fano factor for single units across

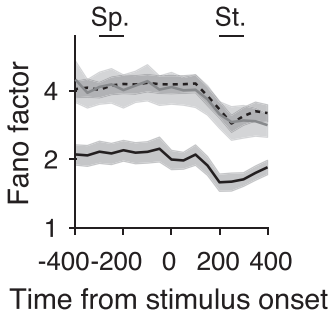

Figure 3. Mean-matched Fano factors in V1-damaged and control animals. Mean-matched Fano factors across the trial for units with receptive fields outside scotoma (black dashed line, $n = 124$ conditions), inside scotoma (gray line, $n = 256$ conditions), and from control animals (black line, $n = 192$ conditions). Error bars indicate 95% confidence intervals. Sp., spontaneous interval; St., stimulus interval.

the trial (see Methods) to estimate whether variability in firing rate changes after loss of V1 input. While units still showed the characteristic dip in Fano factor at stimulus onset (Churchland et al. 2010), Fano factors remained high in the single units from V1-damaged animals. In fact, Fano factors were significantly higher in V1-damaged animals regardless of whether units were inside or outside the LPZ (Fig. 3, Outside LPZ: Spontaneous median = 3.13, $P = 1.0 \times 10^{-14}$; Stimulus median = 2.08, $P = 6.65 \times 10^{-17}$, Wilcoxon's rank sum; Inside LPZ: Spont. median = 2.78, $P = 2.03 \times 10^{-16}$; Stim. median = 2.09, $P = 1.91 \times 10^{-19}$) compared with controls (Spont. median = 1.61; Stim. median = 1.25). In summary, firing rates were both higher and more variable in V1-damaged animals, which may reflect changes in the balance of local excitation (Litwin-Kumar and Doiron 2012), as has been previously observed following loss of sensory input (Keck et al. 2011; Barnes et al. 2017).

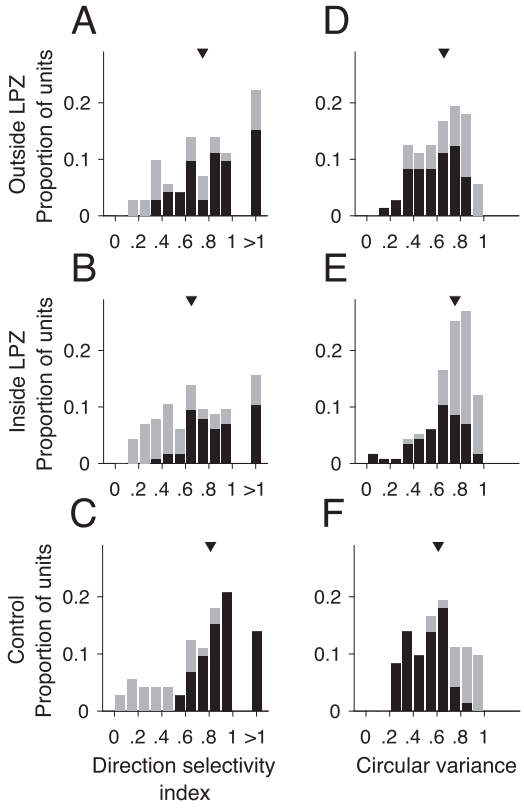

Figure 4. MT units inside LPZ are less direction selective. (A–C) DSI and (D–F) CV for units located outside the LPZ ($n = 72$ units), inside the LPZ ($n = 115$ units), and for the 2 control animals ($n = 72$ units), respectively. Darker bars indicate direction selective units; lighter bars indicate non-direction selective units. Triangles indicate median of distribution.

Neurons in MT Are Less Selective for Direction Following V1 Lesions

To further quantify the directional response in MT, we measured the DSI and CV. Units outside the LPZ in V1-damaged animals did not have significantly lower direction selectivity indices (Fig. 4A, median = 0.74) in comparison with those from control animals (Fig. 4C, Control, median = 0.81, $P = 0.78$, Wilcoxon's rank sum). In comparison, units inside the LPZ had a significantly different distribution of direction indices, which was biased toward low values (Fig. 4B, median = 0.65, $P = 0.02$). Likewise, the CV was significantly higher, indicating reduced direction selectivity for units inside the LPZ compared with units outside the LPZ (Fig. 4D, Outside LPZ: median = 0.66; Fig. 4E, Inside LPZ: median = 0.75, $P = 1.94 \times 10^{-3}$) as well as to control units (Fig. 4F, median = 0.61, $P = 4.83 \times 10^{-5}$). The CV of units outside the LPZ was not significantly different from controls ($P = 0.27$).

These results present a contrast to previous studies, which reported direction selective responses to be largely preserved outside the LPZ shortly after V1 lesions (Rodman et al. 1989; Rosa et al. 2000), and no significant difference in direction selectivity indices for cells inside the LPZ compared with cells in normal MT (Rodman et al. 1989). However, these experiments differed from ours in that they were performed within weeks of V1 damage and used drifting bars and gratings. To ascertain that the difference in our results was due to the time elapsed since the V1 lesion and not the choice of stimuli, we tested the direction selectivity of a subset of neurons in our data set using moving gratings. As with moving dots, few units showed significant direction selective responses (26.1%, 6/23 units). Likewise, firing rates were similar between the preferred and null direction (see Supplementary Fig. S2A, median preferred rate = 18.44 sp/s, median null rate = 12.50 sp/s, $P = 0.88$, Wilcoxon's rank sum). Finally, there was no significant change in the DSI when using dots versus grating (see Supplementary Fig. S2B, median grating DSI = 0.77, $P = 0.09$, Wilcoxon's rank sum). Therefore, we find that direction selective in MT was reduced in the months following V1 lesions irrespective of the stimuli presented.

Impact of V1 Lesions on MT Responses to Motion Coherence

Despite reduced direction selectivity, we found the responses of MT in V1-damaged animals showed surprisingly robust responses to changes in the strength of motion in the stimulus. For typical direction selective MT units, firing rates increase with motion strength (i.e., coherence) in the preferred direction and decrease with motion strength in the null direction (e.g., Fig. 5C, Britten et al. 1992; Chaplin et al. 2017). After V1 lesions, the majority of MT units tested for sensitivity to motion coherence, both direction selective and non-direction selective, did not show the expected monotonic relationship between firing rate and coherence. Instead, units both outside (Fig. 5A) and inside (Fig. 5B) the LPZ showed a "U-shaped" response to changes in

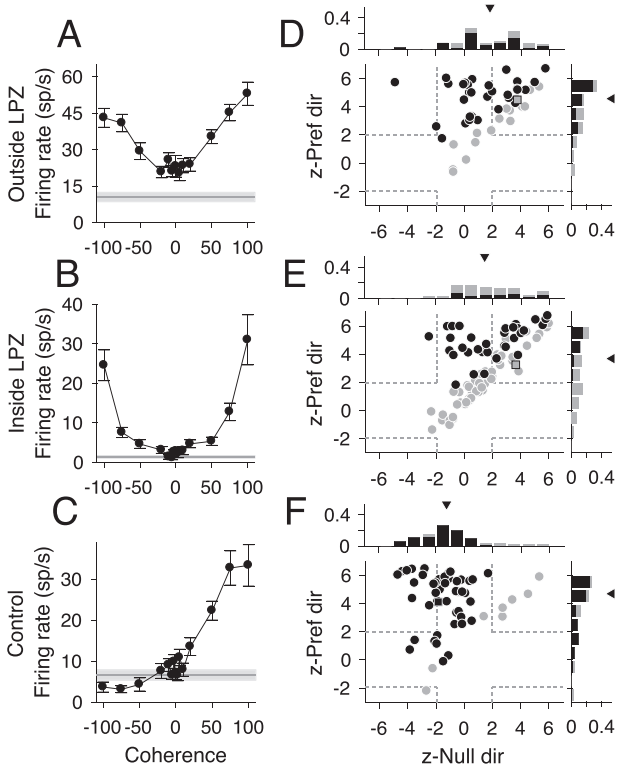

Figure 5. Responses to motion coherence after V1 lesions. (*A–C*) Neural responses from 3 example units (outside the LPZ, inside the LPZ, and from a control animal, respectively) that showed typical responses for each population to motion coherence. Stimulus motion in the preferred direction is indicated by positive coherence values and in the null direction by negative coherence values. Average spontaneous firing rate indicated by the gray line; shaded area indicates standard error. (*D–F*) Scatter plots of z-scored firing rates for units located outside the LPZ ($n = 49$ units), inside the LPZ ($n = 87$ units), and for the control animals ($n = 54$ units), respectively. The *y*-axis shows the z-score for the firing rate difference between a stimulus with 100% coherence in the preferred direction and a stimulus with 0% coherence. The *x*-axis shows the z-score for the firing rate difference between a stimulus with 100% coherence in the null direction and a stimulus with 0% coherence. Each circle represents one unit. Darker circles indicate direction selective units; lighter circles indicate non-direction selective units. Squares indicate example units shown in *A–C*; dashed gray lines indicate the significance threshold for each z-score (+/−1.96). Histograms show the distribution of z-scores for each axis. Triangle indicates median z-scores.

motion coherence, meaning that firing rates were highest for motion at 100% coherence, regardless of stimulus direction.

To quantify this curve shape, we calculated the z-score between firing rates at 100% coherence and 0% coherence for the preferred and null direction. Units with U-shaped responses had significantly positive z-scores (<1.96) for both the preferred and null direction (top right quadrant of Fig. 5*D–F*). Units with traditional linear responses had significantly positive z-scores in the preferred direction and negative z-scores in the null direction (top left quadrant of Fig. 5*D–F*). The majority of units both outside the LPZ (Fig. 5*D*, 43/49, 87.5%, median = 4.53, $P = 0.82$, Wilcoxon's rank sum compared with controls) and inside the LPZ (Fig. 5*E*, 57/87, 65.5%, median = 3.68, $P = 0.02$) showed significant increases in firing rate to the 100% coherent stimulus in the preferred direction, like control animals (Fig. 5*F*, 44/54, 81.5%, median = 4.69). However, unlike controls, a significant percentage of units in V1-damaged animals also showed positive z-scores in the null direction (Outside LPZ: 24/49, 48.9%, median = 1.79, $P = 8.47 \times 10^{-6}$; Inside LPZ: 38/87, 43.6%, median = 1.43, $P = 1.08 \times 10^{-6}$; Control: 5/54, 9.3%, median = −1.25). Notably, this was true for both direction selective and non-direction selective units. Furthermore, this result was consistent when looking at single units alone (see Supplementary Fig. S3*A*, Outside LPZ: Pref. median = 4.65, $P = 0.96$; Null median = 0.60, $P = 7.59 \times 10^{-4}$; see Supplementary Fig. S3*B*, Inside LPZ: Pref. median = 3.87, $P = 0.08$; Null median = 1.46, $P = 2.65 \times 10^{-5}$; see Supplementary Fig. S3*C*, Control: Pref. median = 4.70; Null median = −1.12). Therefore, the majority of MT units in V1-damaged animals were sensitive to motion coherence, regardless of stimulus direction.

Sensitivity to Stimulus Noise Is Impaired after Long-Term V1 Lesions

In macaques, it has been shown that the sensitivity of individual MT units is comparable to human behavioral performance when discriminating direction of noisy, random dot stimuli (Britten et al. 1992). Here, we asked whether the responses of MT units in chronic, V1-damaged animals are consistent with abnormal processing of stimulus noise, as was shown in humans with chronic V1 lesions (Azzopardi and Cowey 2001; Huxlin et al. 2009; Das et al. 2014). We quantified the information carried by the firing rates of each unit by fitting a neurometric function and defining a direction threshold that was the coherence at which the performance was 0.82 (see Methods). Significantly fewer units in V1-damaged animals had direction thresholds (Fig. 6*A*, example unit; Outside LPZ: 19/49, 38.8%, $P = 1.22 \times 10^{-4}$, Fig. 6*B*, example unit; Inside LPZ: 23/87, 26.4%, $P = 2.77 \times 10^{-13}$, Binomial distribution) compared with control animals (Fig. 6*C*, example unit; 35/54, 64.8%). Furthermore, the distribution of direction thresholds was significantly higher for units both outside the LPZ (Fig. 6*D*; median = 0.80, $P = 2.08 \times 10^{-3}$, Wilcoxon's rank sum) and inside the LPZ (Fig. 6*E*, median = 0.79, $P = 7.94 \times 10^{-3}$) in comparison with controls (Fig. 6*F*, median = 0.63). In summary, in line with the reduced direction selectivity, the sensitivity to direction in noise of MT units was substantially reduced in V1-damaged animals.

Given that the majority of units in V1-damaged animals still showed significant increases in firing rate in response to increases in motion coherence, regardless of direction of motion, we next compared the firing rate at each coherence in the preferred direction to the firing rate to the 0% coherence stimulus (Chaplin et al. 2017). This metric calculates the ability of the unit to detect motion, regardless of the direction. As for the direction thresholds, we defined the coherence at which the aROC curve reached 0.82 to be the unit's motion threshold (Fig. 6*G–I*). A greater percentage of units reached the motion threshold compared with the direction threshold, although for units with inside LPZ there were still significantly fewer that reached threshold compared with controls (Outside LPZ: 29/49, 59.2%, $P = 0.06$, Binomial distribution; Inside LPZ: 45/87, 51.7%, $P = 1.37 \times 10^{-3}$; Control: 36/54, 66.7%). The distributions of motion thresholds were also significantly higher than in controls for both units inside and outside the LPZ (Fig. 6*J*, Outside LPZ: median = 0.75, $P = 4.27 \times 10^{-3}$, Wilcoxon's rank sum; Fig. 6*K*, Inside LPZ: median = 0.78, $P = 3.91 \times 10^{-3}$; Fig. 6*L*, Control: median = 0.65). This indicates that the majority of units in animals with V1 lesions retain sensitivity to the strength of motion, regardless of whether the unit is sensitive to the direction of motion.

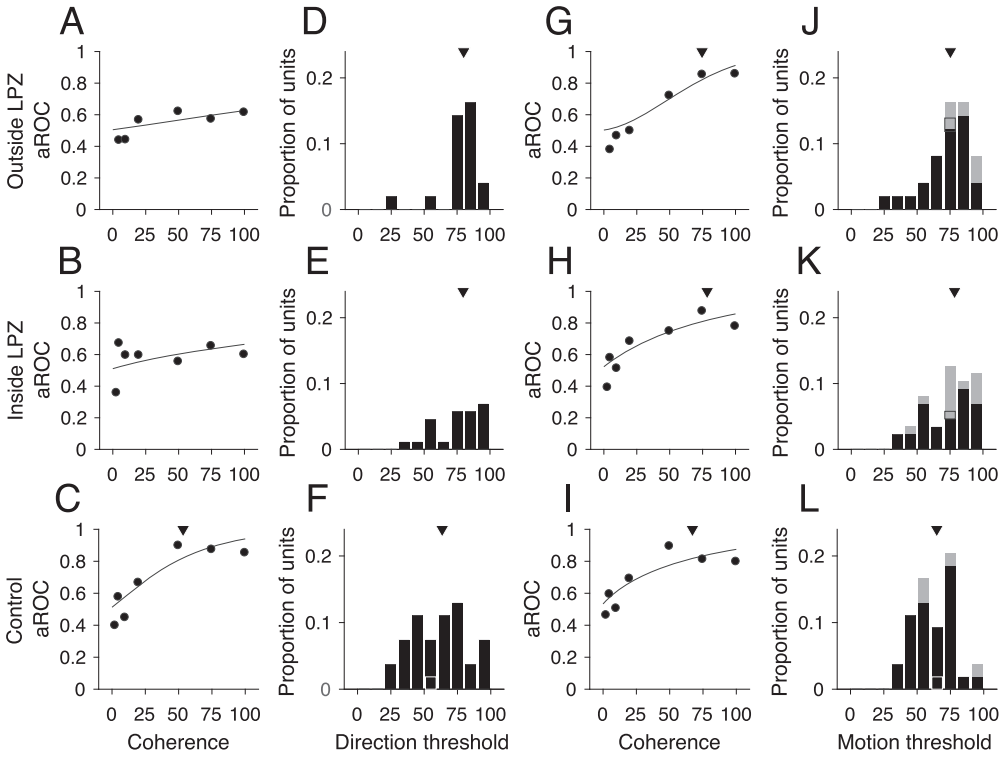

Figure 6. Direction thresholds and motion thresholds. (*A–C*) Neurometric curves, data points indicate aROC values (preferred vs. null response) at each coherence for the same example units shown in Figure 5A–C. The line indicates the best-fitting Weibull curve. Triangle in *C* shows the direction threshold coherence at which the curve reaches an aROC value of 0.82. (*D–F*) Distributions of units with direction thresholds located outside the LPZ ($n = 19/49$ units), inside the LPZ ($n = 23/87$ units), and for the 2 control animals ($n = 35/54$ units), respectively. Black outlines indicate example units shown in A–C. Triangles indicate median threshold for each population. (*G–I*) Neurometric curves, data points indicate aROC values (preferred vs. zero coherence response) at each coherence for same example units shown in Figure 5A–C. All conventions as in A–C. (*J–L*) Distributions of units with motion thresholds located outside the LPZ ($n = 29/49$ units), inside the LPZ ($n = 45/87$ units), and for the 2 control animals ($n = 36/54$ units), respectively. All conventions as in *D–F*.

Effect of E/I Imbalance within MT on Neural Responses

To test whether changes in E/I connections could explain the firing rate changes we observed in MT, we implemented a biophysical network model that has been shown to account for the responses of MT neurons (Wimmer et al. 2015). The model was composed of excitatory and inhibitory, leaky integrate-and-fire neurons, containing 2 excitatory populations (Fig. 7A, E1 and E2) that were tuned to opposite directions of motion. Excitatory and inhibitory populations were reciprocally connected (probability of connection = 0.2). Under balanced E/I conditions, E1 and E2 showed monotonic increases to changes in stimulus coherence in their respective preferred directions (Fig. 7B, mean response for each population), as would be expected under normal conditions in MT. The spontaneous rates in the model under these conditions were also low (Table 2; mean rate ± SD = 2.06 ± 2.34 sp/s), similar to observed MT responses in control animals.

We were then able to create sub-populations of E1 and E2 that were "inside" or "outside" the LPZ by manipulating the probability of excitatory and inhibitory connections. For neurons "inside" the LPZ, inhibitory synapses were reduced and excitatory lateral connections were strengthened, as has been observed experimentally (Darian-Smith and Gilbert 1994; Palagina et al. 2009; Yamahachi et al. 2009; Keck et al. 2011). As a result, the firing rates in spontaneous, preferred, and null firing rates increased significantly compared with control conditions ($P < 0.01$ for all comparisons; see Table 2), as observed experimentally (Fig. 2). The percentage of direction selective neurons decreased significantly, even for neurons outside the LPZ ($P < 0.01$ for all comparisons; see Table 2) as was observed in experimental data (Figs 1, 2 and 4).

Furthermore, as in our experimental data, we found that the model responses under imbalanced E/I conditions, neurons both outside (Fig. 7C) and inside (Fig. 7D) the LPZ showed "U-shaped" responses to motion coherence, unlike the monotonic responses observed in neurons in control conditions (Fig. 7E). We computed the z-scored firing rates for visually responsive neurons at 100% motion coherence in the preferred direction compared with 0% motion coherence and at 100% motion coherence in the null direction compared with 0% coherence (equivalent to the analysis in Fig. 5). Across the population, responses to motion coherence in the null direction significantly increased for neurons both outside the LPZ (Fig. 7F,G, median z-Null dir = 3.72, $P = 7.45 \times 10^{-167}$) and inside the LPZ (Fig. 7G, median z-Null dir = 4.97, $P = 1.81 \times 10^{-254}$; Wilcoxon's rank sum compared with control conditions; Fig. 7H median z-Null dir = −2.59) as was observed experimentally. This indicates that the imbalance E/I inputs generate robust "U-shaped" responses to motion coherence (top right quadrant of Fig. 7F,G). For the control population, where excitatory and inhibitory inputs were balanced, the majority of neurons in the model had z-scores that were significantly positive for the preferred direction (Fig. 7H, 1539/1579, 97.4%, median = 4.48) and negative for the null direction (1082/1579, 68.5%, median = −2.59), indicating

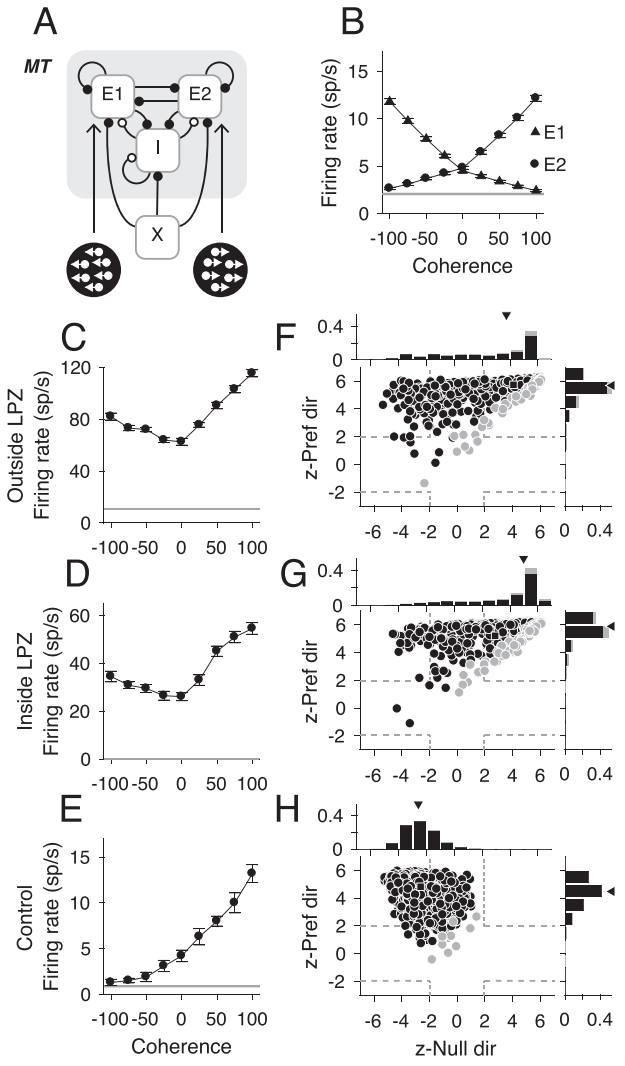

Figure 7. Responses to motion coherence in an imbalanced network model. (*A*) Schematic of network model for an MT-like circuit composed of 2 populations of excitatory neurons (E1, E2) tuned to opposite directions of motion and reciprocally connected inhibitory (I) neurons. Each population receives an external Poisson signal (X). (*B*) Population mean firing rates for E1 neurons (triangles, $n = 800$) and E2 neurons (circles, $n = 800$) in response to varying motion coherence in 2 directions. Gray line indicates mean spontaneous rate; error bars indicate standard error. (*C–E*) Neural responses from 3 example units (inside the LPZ, outside the LPZ, and control, respectively) that showed typical responses for each population to motion coherence. Stimulus motion in the preferred direction is indicated by positive coherence values and in the null direction by negative coherence values. Average spontaneous firing rate indicated by horizontal black lines. Error bars indicate standard error. (*F–H*) Scatter plots of z-scored firing rates for all visually responsive neurons from populations E1 and E2 for each population (Outside LPZ, $n = 530$; Inside LPZ, $n = 679$; and Control, $n = 1579$, respectively). For all scatter plots, the y-axis shows the z-score for the firing rate difference between a stimulus with 100% coherence in the preferred direction and a stimulus with 0% coherence. The x-axis shows the z-score for the firing rate difference between a stimulus with 100% coherence in the null direction and a stimulus with 0% coherence. Each circle represents one simulated neuron. Darker circles indicate direction selective neurons; lighter circles indicate non-direction selective neurons. Squares indicate example neurons shown in *C–E*; dashed gray lines indicate the significance threshold for each z-score (+/−1.96). Histograms show the distribution of z-scores for each axis. Triangle indicates median z-scores.

Table 2 Summary statistics of neural responses from the network model

	Outside LPZ	Inside LPZ	Control
DS neurons	468, 58.5%	592, 74.0%	1564, 97.8%
NDS neurons	62, 7.8%	87, 10.9%	15, 0.94%
NV neurons	270, 33.8%	121, 15.1%	21, 1.31%
Spont. FR	50.42 ± 71.61	65.97 ± 43.88	2.07 ± 2.25
Pref. FR	131.04 ± 71.61	161.31 ± 72.64	12.26 ± 8.60
Null. FR	111.25 ± 75.17	142.18 ± 76.90	2.61 ± 3.34

Control data are out of 1600 neurons, and lesioned data are out of 800 neurons in each subpopulation (800 inside LPZ, 800 outside LPZ). Firing rate summaries show mean ± SD.

highly monotonic responses to motion coherence (top left quadrant of Fig. 7*H*). Because the model represents a simplified network, the variance in the neural responses is less than in the experimental data. The prevalence of direction selectivity in particular is higher in the model than in the experimental data. Nonetheless, the imbalanced E/I inputs replicated the observed long-term effect of V1 lesions on motion coherence in MT units.

We also explored the alternative hypothesis that a change in the input to MT drives the changes in firing rate observed experimentally. The neurons that project from V1 to MT are believed to be direction selective (Movshon and Newsome 1996), but this is not likely to be the case from surviving thalamic inputs (Yu et al. 2018). Therefore, we tested whether the loss of direction selective input alone could account for the changes in neural responses. This manipulation had a little effect on neurons outside the LPZ, which largely still showed monotonic responses to coherence (see Supplementary Fig. S4A and S4B, median z-Pref = 4.86; median z-Null = −1.70), comparable to control conditions. Inside the LPZ, neurons were largely non-direction selective (564/800, 70.5%) and had flat responses to motion coherence (see Supplementary Fig. S4C and S4D, median z-Pref = −0.67; median z-Null = −1.94). Therefore, a change in the direction selective input to the LPZ alone is insufficient to replicate the experimental changes observed.

In summary, by implementing this model, we provide evidence in support of the hypothesis that an imbalance of excitation and inhibition could indeed account for a large number of our physiology results including increased firing rates, reduced direction selectivity, and U-shaped responses to motion coherence regardless of whether neurons were inside or outside the LPZ.

Discussion

In order to understand the long-term consequences of V1 lesions, we recorded responses in MT to moving random dot patterns in adult marmoset monkeys more than 6 months after damage. We found that fewer units in MT were direction selective, regardless of whether they were located inside or outside the LPZ. At the same time, sensitivity to motion coherence was largely preserved, even for a large number of non-direction selective units. Interestingly, the firing rates of the cells were higher and more variable in V1-damaged animals. These observations were explained by reduced input (missing V1 afferents) together with a change in the balance of excitation and inhibition within MT. Together, these results provide novel insights to the underlying mechanisms of neural changes after chronic V1 damage.

Motion Selectivity in MT after Long-Term V1 Lesions

Our data confirmed the long-term preservation of a group of direction selective MT units inside the LPZ, consistent with earlier reports (Rodman et al. 1989; Rosa et al. 2000). However, we found a lower proportion of direction selective cells among the visually responsive units in MT, including units located outside the LPZ compared with previous studies (Rodman et al. 1989; Rosa et al. 2000; Azzopardi et al. 2003), which reported no significant changes to units outside the LPZ. This difference can be accounted for by the longer time scales after V1 lesions used in our study and is consistent with data suggesting that plasticity continues for months post-lesion (Darian-Smith and Gilbert 1994; Giannikopoulos and Eysel 2006; Zhang et al. 2006; Yamahachi et al. 2009). In addition, we observed robust (albeit abnormal) sensitivity to motion coherence, despite the reduced direction selectivity. The increased direction thresholds for noisy moving dot stimuli were also indicative of reduced direction selectivity.

Surprisingly, we found decreased direction selectivity and abnormal sensitivity to motion coherence in neurons located both inside and outside the LPZ. Previous work in adult animals with short-term V1 damage had found neural responses in the region outside the LPZ to be preserved, using bar and square-wave grating stimuli (Rosa et al. 2000). Because MT receptive fields have a finite size (Rosa and Elston 1998), it is likely that neurons near the estimated boundary of the LPZ receive different degrees of input from the remaining parts of V1. Likewise, the receptive fields of many units inside the LPZ tended to be closer to and often overlapped the scotoma border, as has been previously reported following cortical (Eysel and Schweigart 1999; Rosa et al. 2000; Schweigart and Eysel 2002) and retinal lesions (Schmid et al. 1996; Giannikopoulos and Eysel 2006). Thus, the surviving responses inside the LPZ in MT may be dependent on proximity to units outside the LPZ, which still receive inputs from V1, consistent with the notion that direction selectivity in MT may be largely dependent on inputs from V1 (Movshon and Newsome 1996). Together, these results are indicative of potentially widespread changes in the strength of connectivity of units in MT, or at least a substantial change in the balance of inputs previously present, both inside and outside the LPZ, after V1 lesions.

MT Connectivity after V1 Lesions

In addition to inputs from V1 and extrastriate cortical areas, MT also receives direct subcortical input from the koniocellular layers of the lateral geniculate nucleus in both macaques (Sincich et al. 2004) and marmosets (Warner et al. 2010). Many neurons in these layers have "cortical like" response properties (White et al. 2001; Solomon et al. 2010; Cheong et al. 2013), although these properties may be dependent on cortical feedback. MT also receives input from the inferior pulvinar nucleus (Berman and Wurtz 2010, 2011). Both the lateral geniculate nucleus (Bridge et al. 2010; Schmid et al. 2011; Ajina et al. 2015; Yu et al. 2018) and the pulvinar (Rodman et al. 1990; Warner et al. 2012, 2015) have been implicated in the preservation of MT responses after V1 damage. Many neurons in the LPZ of the lateral geniculate nucleus degenerate over the first several months after V1 lesions (Atapour et al. 2017); however, the projections to MT appear to be preserved (Bridge et al. 2008; Ajina et al. 2015), and robust responses have been recorded from all layers of the lateral geniculate nucelus (LGN) after V1 lesion (Yu et al. 2018). Together, these results suggest that subcortical inputs to MT may contribute to residual responses in MT after V1 lesions, particularly for responses observed well inside the LPZ.

Changes in local connectivity may also occur following V1 lesions. Data from retinal lesion models suggest that loss of sensory input can induce rapid changes in neural plasticity (Giannikopoulos and Eysel 2006; Yamahachi et al. 2009; Keck et al. 2011) that can continue for months (Kaas et al. 1990; Darian-Smith and Gilbert 1994; Yamahachi et al. 2009). Shortly after V1 lesions, "bursty" spontaneous rates were reported inside the LPZ (Rodman et al. 1989), which may indicate early changes in the synaptic balance in MT. However, Rodman et al. (1989) reported no change in the overall spontaneous firing rate. Furthermore, shorter-term lesions and temporary inactivation studies of V1 have reported lower firing rates in MT, particularly for units inside the LPZ (Rodman et al. 1989; Girard et al. 1992). Contrary to this, we found higher than normal firing rates (both spontaneous and stimulus-induced) in MT long after V1 damage, suggesting that plasticity may continue to evolve for several months post-lesion. We also found that the Fano factors for MT single units in V1-damaged animals were significantly higher than those of controls. Previous modeling work has suggested that high Fano factors can be achieved via "over clustering" of excitatory responses (Litwin-Kumar and Doiron 2012). It could be that after V1 lesions, the units that remain active become more interconnected with one another, leading to higher variability and broader directional tuning. Previous studies have found that a lack of sensory input decreases the number of inhibitory interneuron synapses (Keck et al. 2011). Within MT, a loss of local inhibition has been shown to decrease direction selectivity (Thiele et al. 2004), consistent with our findings (Fig. 4). Furthermore, cortical hyper-excitability has been observed in V1 following cortical (Barmashenko et al. 2001, 2003; Mittmann and Eysel 2001; Schweigart and Eysel 2002) and retinal (Giannikopoulos and Eysel 2006) lesions. Retinal lesions have been shown to increase molecular activity within the LPZ of MT, indicating increased neural activity (Burnat et al. 2017). This increased excitability may be due to the strengthening of excitatory lateral connections from within the LPZ and from neighboring cortical areas, as has been observed after loss of sensory input (Kaas et al. 1990; Darian-Smith and Gilbert 1994; Palagina et al. 2009; Yamahachi et al. 2009). In the weeks following V1 lesions, long-term potentiation is enhanced near the lesion border (Mittmann and Eysel 2001; Barmashenko et al. 2003), driven by increases in intracellular calcium signaling (Barmashenko et al. 2001, 2003). Together, these results suggest that adult cortex is primed for facilitating neural plasticity following cortical lesions.

Consistent with this, an E/I imbalance driven by increased strength of excitatory lateral interactions and decreased probability of inhibitory synapses could explain the observed decreased direction selectivity and increased firing rates. The "U-shaped" responses to motion coherence were captured when neurons inside the LPZ received either direction selective or non-visual input. This model was chosen as it allowed for the manipulation of parameters associated with these neural mechanisms (Wimmer et al. 2015). The differences between the modelled (Fig. 7) and the experimental (Fig. 5) data point to the inevitable fact that the neural mechanisms post-lesion are not limited to those identified by the modeling alone. For example, the variance of response to the null direction in the experimental data is greater. If indeed a disrupted E/I balance is the mechanism that underlies this effect, it is likely

that there is great variability in the degree of plasticity that individual neurons undergo. The model does not incorporate this potential variability. It is also likely that there is diversity in the source input to individual neurons inside the LPZ. Our results suggest that a loss of direction selective input in the LPZ alone is insufficient to explain our experimental findings (see Supplementary Fig. S4). However, it is likely that variability in the inputs to the LPZ, together with variability in the degree of plasticity across neurons, contributes to the variance observed in the experimental data.

Finally, the model was agnostic to the origin of input into the LPZ of MT. Direction selective inputs into units near the LPZ boundary may still come from surviving V1 (Hagan et al. 2017). In support of this, following V1 lesions, some neurons in V1 along the lesion border increase their receptive field size (Eysel and Schweigart 1999; Schweigart and Eysel 2002), likely utilizing the lateral spread of geniculocortical connections (Gilbert and Wiesel 1979). Units recorded from inside LPZ had receptive fields that overlapped the scotoma boundary (Eysel and Schweigart 1999; Schweigart and Eysel 2002; Fig. 1A–D). Direction selectivity may also be generated within MT from non-directional inputs (Rodman et al. 1989; Girard et al. 1992) or from weakly direction selective lateral geniculate nucleus (LGN) neurons (White et al. 2001; Cheong et al. 2013). Furthermore, the model does not investigate how the network may become imbalanced. Such imbalance may occur directly after loss of sensory input or slowly through an adaptive learning process. However, data from other animal models suggest that these changes can be quite rapid (Giannikopoulos and Eysel 2006; Yamahachi et al. 2009; Keck et al. 2011). Nonetheless, our simplified network demonstrates that a change in the E/I balance can account for changes in MT responses after V1 lesion.

Implications for Adult Humans with V1 Damage

Patients who suffer damage to V1 usually experience a period of spontaneous behavioral recovery, which may last up to 6 months (Zhang et al. 2006). The majority of hemianopic studies characterize behavioral performance after this period, when the visual field defect has stabilized. The results of the present study, performed more than 6 months post-lesion, provide the most meaningful comparisons to date between non-human primate MT physiology and the behavioral performance of chronic hemianopic patients. The only previous study performed on a similar timescale found no visual responses inside the scotoma of New World monkeys (Collins et al. 2003), a result that may be linked to the use of different anesthetics (Girard et al. 1992) and purely qualitative assessment of responsiveness. We also found a high percentage of units that were unresponsive to our stimulus, consistent with findings in V1 after retinal lesions (Giannikopoulos and Eysel 2006). These units would likely have had receptive fields inside the scotoma before the lesion based on their anatomical location within MT.

Chronic hemianopic patients cannot easily discriminate the direction of motion of random dot stimuli (Azzopardi and Cowey 2001), a result that correlates well with the poor direction selectivity we observed in similar conditions. However, recent studies have found that perceptual training can improve motion discrimination in such patients (Sahraie et al. 2006, 2010; Raninen et al. 2007; Huxlin et al. 2009; Das et al. 2014; Cavanaugh et al. 2015; Cavanaugh and Huxlin 2017), including back to normal levels of performance (Cavanaugh and Huxlin 2017). For this to occur, there must be neurons with sufficient motion encoding that can be recruited for perception. The robust sensitivity to motion coherence we found in our data and the remaining direction selective cells suggest that MT is a likely site to mediate these perceptual improvements. The responses we recorded along the border of the scotoma are also consistent with the finding that functional recovery with perceptual training in patients with chronic V1 lesions occurs primarily at the edges of the scotoma (Cavanaugh and Huxlin 2017; Barbot et al. 2018). Experimentally, perceptual training has been shown to increase receptive field size in cells along the LPZ border (Schweigart and Eysel 2002).

Taken together, our findings demonstrate that the rudiments of motion processing persist in area MT of marmosets with long-standing V1 lesions. The functional changes we observed are consistent with long-term changes in the structural inputs into MT neurons. These changes may provide the infrastructure for continued motion perception. Furthermore, our results suggest that MT remains a very likely neural substrate for training-induced improvements in motion perception that can be elicited in chronic hemianopic patients. Indeed, one would predict that the sensitivity of MT neurons to random dot patterns would improve during perceptual training.

Supplementary Material

Supplementary material is available at *Cerebral Cortex* online.

Funding

Australian Research Council (grant DE180100344 to M.H., grant DE130100493 to L.L., and grant CE140100007 to M.R.); National Health and Medical Research Council of Australia (grant APP1066232 to L.L., grant APP1083152 to M.R., and grant APP1159764 to T.C.); Monash University Faculty of Medicine Bridging Postdoctoral Fellowship (to T.C.); Research to Prevent Blindness Foundation to the Flaum Eye Institute (to K.R.H.); National Institute of Health (NIH) (grants EY027314 and EY021209 to K.R.H.).

Notes

We thank Katrina Worthy for the histological work. We also thank Janssen-Cilag for the donation of sufentanil citrate that made some of our experiments possible. *Conflict of Interest*: None declared.

References

Ajina S, Pestilli F, Rokem A, Kennard C, Bridge H. 2015. Human blindsight is mediated by an intact geniculo-extrastriate pathway. *Elife*. 4:1–23.

Alexander I, Cowey A. 2008. The cortical basis of global motion detection in blindsight. *Exp Brain Res*. 192:407–411.

Atapour N, Worthy KH, Lui LL, Yu H-H, Rosa MGP. 2017. Neuronal degeneration in the dorsal lateral geniculate nucleus following lesions of primary visual cortex: comparison of young adult and geriatric marmoset monkeys. *Brain Struct Funct*. 222:3283–3293.

Azzopardi P, Cowey A. 2001. Motion discrimination in cortically blind patients. *Brain*. 124:30–46.

Azzopardi P, Fallah M, Gross CG, Rodman HR. 2003. Response latencies of neurons in visual areas MT and MST of monkeys with striate cortex lesions. *Neuropsychologia*. 41:1738–1756.

Barbot A, Melnick M, Cavanaugh M, Das A, Merriam E, Heeger D, Huxlin K. 2018. Visual recovery in chronic cortically-blind patients relies on spared cortical activity and increased V1 coverage of the blind field. *J Vis*. 18:1074.

Barbur JL, Watson JDG, Frackowiak RSJ, Zeki S. 1993. Conscious visual perception without VI. *Brain*. 116:1293–1302.

Barmashenko G, Eysel UT, Mittmann T. 2001. Intracellular calcium signals in the surround of rat visual cortex lesions. *Neuroreport*. 12:3023–3028.

Barmashenko G, Eysel UT, Mittmann T. 2003. Changes in intracellular calcium transients and LTP in the surround of visual cortex lesions in rats. *Brain Res*. 990:120–128.

Barnes SJ, Franzoni E, Jacobsen RI, Erdelyi F, Szabo G, Clopath C, Keller GB, Keck T. 2017. Deprivation-induced homeostatic spine scaling in vivo is localized to dendritic branches that have undergone recent spine loss. *Neuron*. 96:871–882.

Berman RA, Wurtz RH. 2010. Functional identification of a pulvinar path from superior colliculus to cortical area MT. *J Neurosci*. 30:6342–6354.

Berman RA, Wurtz RH. 2011. Signals conveyed in the pulvinar pathway from superior colliculus to cortical area MT. *J Neurosci*. 31:373–384.

Brainard DH. 1997. The Psychophysics Toolbox. *Spat Vis*. 10:433–436.

Bridge H, Hicks SL, Xie J, Okell TW, Mannan S, Alexander I, Cowey A, Kennard C. 2010. Visual activation of extra-striate cortex in the absence of V1 activation. *Neuropsychologia*. 48: 4148–4154.

Bridge H, Thomas O, Jbabdi S, Cowey A. 2008. Changes in connectivity after visual cortical brain damage underlie altered visual function. *Brain*. 131:1433–1444.

Britten KH, Shadlen MN, Newsome WT, Movshon JA. 1992. The analysis of visual motion: a comparison of neuronal and psychophysical performance. *J Neurosci*. 12:4745–4765.

Burnat K, Hu T-T, Kossut M, Eysel UT, Arckens L. 2017. Plasticity beyond V1: reinforcement of motion perception upon binocular central retinal lesions in adulthood. *J Neurosci*. 37:8989–8999.

Cavanaugh MR, Huxlin KR. 2017. Visual discrimination training improves Humphrey perimetry in chronic cortically induced blindness. *Neurology*. 88:1856–1864.

Cavanaugh MR, Zhang R, Melnick MD, Das A, Roberts M, Tadin D, Carrasco M, Huxlin KR. 2015. Visual recovery in cortical blindness is limited by high internal noise. *J Vis*. 15:9.

Chaplin TA, Allitt BJ, Hagan MA, Price NSC, Rajan R, Rosa MGP, Lui LL. 2017. Sensitivity of neurons in the middle temporal area of marmoset monkeys to random dot motion. *J Neurophysiol*. 118:1567–1580.

Chaplin TA, Yu H-H, Rosa MGP. 2013. Representation of the visual field in the primary visual area of the marmoset monkey: magnification factors, point-image size, and proportionality to retinal ganglion cell density. *J Comp Neurol*. 521: 1001–1019.

Cheong SK, Tailby C, Solomon SG, Martin PR. 2013. Cortical-like receptive fields in the lateral geniculate nucleus of marmoset monkeys. *J Neurosci*. 33:6864–6876.

Churchland MM, Yu BM, Cunningham JP, Sugrue LP, Cohen MR, Corrado GS, Newsome WT, Clark AM, Hosseini P, Scott BB *et al*. 2010. Stimulus onset quenches neural variability: a widespread cortical phenomenon. *Nat Neurosci*. 13:369–378.

Collins CE, Lyon DC, Kaas JH. 2003. Responses of neurons in the middle temporal visual area after long-standing lesions of the primary visual cortex in adult new world monkeys. *J Neurosci*. 23:2251–2264.

Darian-Smith C, Gilbert CD. 1994. Axonal sprouting accompanies functional reorganization in adult cat striate cortex. *Nature*. 368:737–740.

Das A, Tadin D, Huxlin KR. 2014. Beyond blindsight: properties of visual relearning in cortically blind fields. *J Neurosci*. 34:11652–11664.

Eysel UT, Schweigart G. 1999. Increased receptive field size in the surround of chronic lesions in the adult cat visual cortex. *Cereb Cortex*. 9:101–109.

Eysel UT, Schweigart G, Mittmann T, Eyding D, Qu Y, Vandesande F, Orban G, Arckens L. 1999. Reorganization in the visual cortex after retinal and cortical damage. *Restor Neurol Neurosci*. 15:153–164.

Fritsches KA, Rosa MGP. 1996. Visuotopic organisation of striate cortex in the marmoset monkey (Callithrix jacchus). *J Comp Neurol*. 372:264–282.

Gallyas F. 1979. Silver staining of myelin by means of physical development. *Neurol Res*. 1:203–209.

Giannikopoulos DV, Eysel UT. 2006. Dynamics and specificity of cortical map reorganization after retinal lesions. *Proc Natl Acad Sci U S A*. 103:10805–10810.

Gilbert CD, Wiesel TN. 1979. Morphology and intracortical projections of functionally characterised neurones in the cat visual cortex. *Nature*. 280:120–125.

Girard P, Salin PA, Bullier J. 1992. Response selectivity of neurons in area MT of the macaque monkey during reversible inactivation of area V1. *J Neurophysiol*. 67:1437–1446.

Hagan MA, Rosa MGP, Lui LL. 2017. Neural plasticity following lesions of the primate occipital lobe: the marmoset as an animal model for studies of blindsight. *Dev Neurobiol*. 77: 314–327.

Horton JC, Hoyt WF. 1991. The representation of the visual field in human striate cortex. A revision of the classic Holmes map. *Arch Ophthalmol*. 109:816–824.

Huxlin KR, Martin T, Kelly K, Riley M, Friedman DI, Burgin WS, Hayhoe M. 2009. Perceptual relearning of complex visual motion after V1 damage in humans. *J Neurosci*. 29: 3981–3991.

Kaas JH, Krubitzer LA, Chino YM, Langston AL, Polley EH, Blair N. 1990. Reorganization of retinotopic cortical maps in adult mammals after lesions of the retina. *Science*. 248:229–231.

Kaas JH, Lyon DC. 2007. Pulvinar contributions to the dorsal and ventral streams of visual processing in primates. *Brain Res Rev*. 55:285–296.

Keck T, Scheuss V, Jacobsen RI, Wierenga CJ, Eysel UT, Bonhoeffer T, Hübener M. 2011. Loss of sensory input causes rapid structural changes of inhibitory neurons in adult mouse visual cortex. *Neuron*. 71:869–882.

Klüver H. 1936. An analysis of the effects of the removal of the occipital lobes in monkeys. *J Psychol*. 2:49–61.

Klüver H. 1941. Visual functions after removal of the occipital lobes. *J Psychol*. 11:23–45.

Lister WT, Holmes G. 1916. Disturbances of vision from cerebral lesions, with special reference to the cortical representation of the macula. *Proc R Soc Med*. 9:57–96.

Litwin-Kumar A, Doiron B. 2012. Slow dynamics and high variability in balanced cortical networks with clustered connections. *Nat Neurosci*. 15:1498–1505.

Mittmann T, Eysel UT. 2001. Increased synaptic plasticity in the surround of visual cortex lesions in rats. *Neuroreport*. 12:3341–3347.

Movshon JA, Newsome WT. 1996. Visual response properties of striate cortical neurons projecting to area MT in macaque monkeys. *J Neurosci*. 16:7733–7741.

Palagina G, Eysel UT, Jancke D. 2009. Strengthening of lateral activation in adult rat visual cortex after retinal lesions captured with voltage-sensitive dye imaging in vivo. *Proc Natl Acad Sci U S A*. 106:8743–8747.

Palmer SM, Rosa MGP. 2006. A distinct anatomical network of cortical areas for analysis of motion in far peripheral vision. *Eur J Neurosci*. 24:2389–2405.

Pelli DG. 1997. The VideoToolbox software for visual psychophysics: transforming numbers into movies. *Spat Vis*. 10:437–442.

Poppel E, Held R, Frost D. 1973. Residual visual function after brain wounds involving the central visual pathways in man. *Nature*. 243:295–296.

Raninen A, Vanni S, Hyvarinen L, Nasanen R. 2007. Temporal sensitivity in a hemianopic visual field can be improved by long-term training using flicker stimulation. *J Neurol Neurosurg Psychiatry*. 78:66–73.

Riddoch G. 1917. Dissociation of visual perceptions due to occipital injuries, with especial reference to appreciation of movement. *Brain*. 40:15–57.

Ringach DL, Shapley RM, Hawken MJ. 2002. Orientation selectivity in macaque V1: diversity and laminar dependence. *J Neurosci*. 22:5639–5651.

Rodman HR, Gross CG, Albright TD. 1989. Afferent basis of visual response properties in area MT of the macaque. I. Effects of striate cortex removal. *J Neurosci*. 9:2033–2050.

Rodman HR, Gross CG, Albright TD. 1990. Afferent basis of visual response properties in area MT of the macaque. II. Effects of superior colliculus removal. *J Neurosci*. 10:1154–1164.

Rosa MGP, Elston GN. 1998. Visuotopic organisation and neuronal response selectivity for direction of motion in visual areas of the caudal temporal lobe of the marmoset monkey (Callithrix jacchus): middle temporal area, middle temporal crescent, and surrounding cortex. *J Comp Neurol*. 393:505–527.

Rosa MGP, Tweedale R, Elston GN. 2000. Visual responses of neurons in the middle temporal area of new world monkeys after lesions of striate cortex. *J Neurosci*. 20:5552–5563.

Sahraie A, Hibbard PB, Trevethan CT, Ritchie KL, Weiskrantz L. 2010. Consciousness of the first order in blindsight. *Proc Natl Acad Sci U S A*. 107:21217–21222.

Sahraie A, Trevethan CT, MacLeod MJ, Murray AD, Olson JA, Weiskrantz L. 2006. Increased sensitivity after repeated stimulation of residual spatial channels in blindsight. *Proc Natl Acad Sci U S A*. 103:14971–14976.

Sanders MD, Warrington EK, Marshall J, Wieskrantz L. 1974. "Blindsight": vision in a field defect. *Lancet*. 1:707–708.

Schmid LM, Rosa MGP, Calford MB, Ambler JS. 1996. Visuotopic reorganization in the primary visual cortex of adult cats following monocular and binocular retinal lesions. *Cereb Cortex*. 6:388–405.

Schmid MC, Mrowka SW, Turchi J, Saunders RC, Wilke M, Peters AJ, Ye FQ, Leopold DA. 2011. Blindsight depends on the lateral geniculate nucleus. *Nature*. 466:373–377.

Schmid MC, Schmiedt JT, Peters AJ, Saunders RC, Maier A, Leopold DA. 2013. Motion-sensitive responses in visual area V4 in the absence of primary visual cortex. *J Neurosci*. 33:18740–18745.

Schweigart G, Eysel UT. 2002. Activity-dependent receptive field changes in the surround of adult cat visual cortex lesions. *Eur J Neurosci*. 15:1585–1596.

Sincich LC, Park KF, Wohlgemuth MJ, Horton JC. 2004. Bypassing V1: a direct geniculate input to area MT. *Nat Neurosci*. 7:1123–1128.

Solomon SG, Tailby C, Cheong SK, Camp AJ. 2010. Linear and nonlinear contributions to the visual sensitivity of neurons in primate lateral geniculate nucleus. *J Neurophysiol*. 104:1884–1898.

Stepniewska I, Ql HX, Kaas JH. 2000. Projections of the superior colliculus to subdivisions of the inferior pulvinar in New World and Old World monkeys. *Vis Neurosci*. 17:529–549.

Stettler DD, Das A, Bennett J, Gilbert CD. 2002. Lateral connectivity and contextual interactions in macaque primary visual cortex. *Neuron*. 36:739–750.

Thiele A, Distler C, Korbmacher H, Hoffmann K-P. 2004. Contribution of inhibitory mechanisms to direction selectivity and response normalization in macaque middle temporal area. *Proc Natl Acad Sci U S A*. 101:9810–9815.

Warner CE, Goldshmit Y, Bourne JA. 2010. Retinal afferents synapse with relay cells targeting the middle temporal area in the pulvinar and lateral geniculate nuclei. *Front Neuroanat*. 4:8.

Warner CE, Kwan WC, Bourne JA. 2012. The early maturation of visual cortical area MT is dependent on input from the retinorecipient medial portion of the inferior pulvinar. *J Neurosci*. 32:17073–17085.

Warner CE, Kwan WC, Wright D, Johnston LA, Egan GF, Bourne JA. 2015. Preservation of vision by the pulvinar following early-life primary visual cortex lesions. *Curr Biol*. 25:424–434.

Weiskrantz L. 1996. Blindsight revisited. *Curr Opin Neurobiol*. 6:215–220.

Weller RE, Wall JT, Kaas JH. 1984. Cortical connections of the middle temporal visual area (MT) and the superior temporal cortex in owl monkeys. *J Comp Neurol*. 228:81–104.

White AJ, Solomon SG, Martin PR. 2001. Spatial properties of koniocellular cells in the lateral geniculate nucleus of the marmoset Callithrix jacchus. *J Physiol*. 533:519–535.

Wimmer K, Compte A, Roxin A, Peixoto D, Renart A, de la Rocha J. 2015. Sensory integration dynamics in a hierarchical network explains choice probabilities in cortical area MT. *Nat Commun*. 6:6177.

Yamahachi H, Marik SA, McManus JNJ, Denk W, Gilbert CD. 2009. Rapid axonal sprouting and pruning accompany functional reorganization in primary visual cortex. *Neuron*. 64:719–729.

Yu H-H, Atapour N, Chaplin TA, Worthy KH, Rosa MGP. 2018. Robust visual responses and normal retinotopy in primate lateral geniculate nucleus following long-term lesions of striate cortex. *J Neurosci*. 38:3955–3970.

Yu H-H, Chaplin TA, Egan GW, Reser DH, Worthy KH, Rosa MGP. 2013. Visually evoked responses in extrastriate area MT after lesions of striate cortex in early life. *J Neurosci*. 33:12479–12489.

Yu H-H, Rosa MGP. 2010. A simple method for creating wide-field visual stimulus for electrophysiology: mapping and analyzing receptive fields using a hemispheric display. *J Vis*. 10:15.

Yu H-H, Verma R, Yang Y, Tibballs HA, Lui LL, Reser DH, Rosa MGP. 2010. Spatial and temporal frequency tuning in striate cortex: functional uniformity and specializations related to receptive field eccentricity. *Eur J Neurosci*. 31: 1043–1062.

Zhang X, Kedar S, Lynn MJ, Newman NJ, Biousse V. 2006. Natural history of homonymous hemianopia. *Neurology*. 66: 901–905.